chemosensors

MDPI

Article

Sensing Alzheimer's Disease Utilizing Au Electrode by Controlling Nano-restructuring

Chih-Hsien Hsu [1], Akhilesh Kumar Gupta [2], Agnes Purwidyantri [3,5], Briliant Adhi Prabowo [4,5], Ching-Hsiang Chen [6], Chi-Cheng Chuang [7,8], Ya-Chung Tian [9,*], Yu-Jen Lu [7,8,10,*] and Chao-Sung Lai [1,9,11,12,13,*]

1 Department of Electronic Engineering, Chang Gung University, Taoyuan, Taiwan; jason0419@hotmail.com
2 Graduate Institute of Biomedical Engineering, National Chung Hsing University, Taichung, Taiwan; akhileshddu@gmail.com
3 Research Unit for Clean Technology, National Research and Innovation Agency, Bandung, Indonesia; agnes.purwidyantri@gmail.com
4 Research Center for Electronics and Telecommunications, National Research and Innovation Agency, Bandung, Indonesia; briliant.prabowo@inl.int
5 International Iberian Nanotechnology Laboratory, Braga, Portugal
6 Sustainable Energy Development Center, National Taiwan University of Science and Technology, Taipei, Taiwan; bluse.chen@gmail.com
7 Devision of Neurosurgery, Chang Gung Memorial Hospital, Taoyuan, Taiwan; ccc2915@cgmh.org.tw
8 College of Medicine, Chang Gung University, Taoyuan, Taiwan
9 Department of Nephrology, Chang Gung Memorial Hospital, Linkou, Taiwan
10 Center for Biomedical Science and Engineering, National Tsing Hua University, Hsinchu, Taiwan
11 Biomedical Research Center, Chang Gung University, Taoyuan, Taiwan
12 Department of Materials Engineering, Ming-Chi University of Technology, New Taipei City, Taiwan
13 Artificial Intelligent Research Center, Chang Gung University, Taoyuan, Taiwan
* Correspondence: dryctian@adm.cgmh.org.tw (Y.-C.T.); alexlu0416@gmail.com (Y.-J.L.), cslai@mail.cgu.edu.tw (C.-S.L.)

Citation: Hsu, C.-H.; Gupta, A.K.; Purwidyantri, A.; Prabowo, B.A.; Chen, C.-H.; Chuang, C.-C.; Tian, Y.-C.; Lu, Y.-J.; Lai, C.-S. Sensing Alzheimer's Disease Utilizing Au Electrode by Controlling Nanorestructuring. *Chemosensors* **2022**, *10*, x. https://doi.org/10.3390/xxxxx

Academic Editor(s):

Received: date
Accepted: date
Published: date

Publisher's Note: MDPI stays neutral with regard to jurisdictional claims in published maps and institutional affiliations.

Abstract: This paper reports the development of Alzheimer's disease (AD) sensor through early detection of amyloid-beta (Aβ) (1-42) using simple nanorestructuring of Au sheet plate by oxidation-reduction cycle (ORC) via the electrochemical system. The topology of Au substrates was enhanced through the roughening and Au grains grown by a simple ORC technique in aqueous solutions containing 0.1 mol/L KCl electrolytes. The roughened substrate was then functionalized with the highly specific antibody β-amyloid Aβ (1-28) through HS-PEG-NHS modification, which enabled effective and direct detection of Aβ (1–42) peptide. The efficacy of the ORC method had been exhibited in the polished Au surface by approximately 15% larger electro-active sites compared to the polished Au without ORC. The ORC polished structure demonstrated a rapid, accurate, precise, reproducible, and highly sensitive detection of Aβ (1-42) peptide with a low detection limit of 10.4 fg/mL and a wide linear range of 10^{-2} to 10^{6} pg/mL. The proposed structure had been proven to have potential as an early-stage Alzheimer's disease (AD) detection platform with low-cost fabrication and ease of operation.

Keywords: oxidation-reduction cycles (ORC); nanorestructuring; Au electrode roughening; β-amyloid; Alzheimer's Disease; electrochemical sensor

1. Introduction

Nowadays, the fast-increasing elderly population is an essential medical issue in developed countries, and due to the aging factor, Alzheimer's disease (AD) is rapidly expanding worldwide [1–3]. AD is a simple neurodegenerative syndrome described by memory loss and cognitive failure. As per previous reports, nearly 47 million people worldwide suffer from AD, and the prediction is that four times that number of people will have the condition by the year 2050 [4,5]. From survey studies, the percentage of

aged persons (≥65 years old) in the total population in Taiwan has risen continuously over the past three decades, from 4.1% in 1980 to 10.7% in 2010 [1,6]. AD is the most frequent cause of dementia and has been estimated to cause approximately 60% to 70% of dementia cases in Taiwan [7,8]. In addition, the cost of medical care, which is the highest in brain-related medical conditions in Europe with € 106 billion and $ 236 billion in the US, reflects the economic and communal impact [9].

Several clinical trials have shown that β-amyloid (Aβ) and tau protein are feasible biomarkers that can be used for diagnosing AD in cerebrospinal fluid (CSF) [10,11]. However, neuron loss and the progressive accumulation in neurotic (senile) plaques and blood vessel walls of paired helical filament (PHF), such as Neurofibrillary tangling (NFT), are essential factors. Furthermore, a peptide made up of amino acid residue, called an β-amyloid -peptide (Aβ), consists of a sequence cleavage of β and β-secretase amyloid precursor protein (APP) (39−42) and is the most prevalent element of neurotic plaques [12]. Besides, insoluble aggregates of the β-amyloid peptides Aβ (1−42) and Aβ (1−40), which have been shown to be associated with Alzheimer's illness, are notably generated [13]. The higher level of the peptides marks significant illness progress in AD patients, and hence, the detection based on biomarkers employing such peptides would be decisive in early diagnostics [14]. Due to the progressive loss of cognitive function and expensive care environment for neurodegenerative patients, the early onset of AD should be seriously considered [15].

Current diagnostic methods mainly rely on neuroimaging techniques, such as magnetic resonance imaging (MRI) and amyloid positron emission tomography (PET). However, these methods have many constraints and are not cost-effective [16,17]. More importantly, these instruments typically only detect the later visible stage of AD, such as when the amyloid-beta protein lumps grow and block some parts of the brain. Thus, even though AD is not a curable disease, early detection at the molecular level of protein secretion is urgently required to decide the best treatment for neurodegenerative loss delay in the diagnosed patients [18,19]. In liquid-based molecular detection, biosensors have significantly been considered as a remarkable breakthrough in various medical scenes pertaining to their miniaturized, selective and specific screening. Nevertheless, the available surface area for the effective binding interaction between the probe molecules and their targets is still a significant issue [20]. Among various strategies, the engineering of the sensing surface structure has been tremendously targeted to achieve an effective surface area for the effective confinement of biomolecules generating signal amplification.

A myriad of techniques in nanopatterning for higher surface area generation have been reported. Lithography techniques performed in a standard cleaning room have always been enticing for submicron grafting and high aspect ratio. Nevertheless, the pricey high-end instrumentations, along with the requirement of highly skilled technicians, have made it difficult to realize within the tight budget of sensor development. It should be underlined that a future where biosensors are cheap and accessible would favor society. As a reliable and straightforward alternative, the electrochemical roughening pathway has been widely applied in surface topology engineering, such as through template synthesis [21], chemical dealloying [22], electrochemical deposition [23], electrochemical erosion [24], and repetitive square-wave oxidation-reduction cycle (SWORC) [25], electroplating or electrodeposition. However, in some of those protocols, for instance, in electrochemical deposition or electroplating, despite its simple and quick process, as reported by Asnavandi et al., due to limited electron transfer from the catalyst to substrate, some additional chemical binders such as Nafion or hydrophobic polytetrafluoroethylene (PTFE) are somehow needed. Thus, more steps are required in the whole procedure as well as the elimination of the risk of peel-off [26]. It is also noted that the chemical binder also affects the reduction in active surface sites during measurement [27].

From the various electrochemical-based methods mentioned above, the electrochemical oxidation-reduction cycle is noticeably economical, simple, and environmen-

tally friendly since 3D roughened film can be tuned easily, without any additional treatments, solely by controlling the continuous repetition of gold oxidation-reduction and hydrogen evolution into the system [28,29]. Liu et al. reported a successful ORC technique using 0.1 M KCl solution with many differentiations in anodic and cathodic scan rates, delays, and cycle times to obtain a roughed Au structure for polypyrrole Raman study [30]. Interestingly, Bailey et al. reported the incredible impact of replacing the traditional use of chloride with NaOH in Ag roughening for SERS substrate preparation, resulting in a high degree of roughness, effective for SERS screening [31]. Apart from Raman spectroscopy studies' application, which mainly uses unique plasmonic effects from the roughened substrate [32,33], the ORC-engineered conductive substrate with its vast active area is potentially applied for other sensing platforms, such as in electrochemical sensors.

Here in this work, we are the first to demonstrate a facile single-step nanorestructuring strategy for preparing a large area of high surface roughened Au electrode, without any additional capping agents, using the ORC technique to build up an electrochemical sensor. As proof of concept, the ORC engineered Au substrate was functionalized by the HS-PEG-NHS linker and utilized to detect AD biomarker, Aβ (1-42) peptide, in a wide dynamic range favoring an early detection diagnosis of AD. Outcomes denoted that ORC-restructured Au electrode paves a path toward tunable nano-patterning with excellent topology for high throughput and at a low-cost process, which also opens a niche targeting various applications including field-effect transistors (FETs) and optical-based biosensors, LEDs-based platforms, solar-cells, advanced sensors, and microelectronics.

2. Materials and Experimental Methods

2.1. Materials

Gold electrode sheet was purchased from CL Technology Co. Ltd. (Taiwan). Acetone, Isopropyl alcohol (IPA), and toluene were purchased from Avantor (PA, USA). The polishing pad was purchased from LECO Corporation (USA). HS-PEG-NHS (2K) was purchased from Nanocs (USA). Aβ (1-28) antibody and Aβ (1-42) peptide were purchased from Abiotic (USA). Phosphate buffered saline (PBS) was purchased from Sigma-Aldrich (USA). The experimental solutions were prepared using deionized 18.2 MΩ water produced by a MilliQ system. Potassium chloride was purchased from Merck (Darmstadt, Germany).

2.2. Apparatus

The morphological images of Au electrode with and without polishing treatment altogether with the impact of ORC were characterized using a field emission scanning electron microscopy combined with energy-dispersive spectroscopy (FE-SEM, EDS) JEOL-JSM-7500 F (Pleasanton, CA, USA). Atomic force microscopy (AFM) Innova B067-Bruker Corp (Camarillo, CA, USA) and the total area of AFM tapping mode 100 μm^2 with scan rate were applied to analyze the surface topology of the engineered substrate at 0.1 Hz and with 512 resolution. Cyclic voltammetry (CV) was conducted using a three-electrode system 611E Electrochemical Analyzer from CH Instruments, Inc. (Austin, TX, USA).

2.3. ORC Nanorestructuring of Au Substrate

Firstly, the initial gold sheet was automatically polished by polishing pads employing different sizes of alumina powder (0.1 μm and 0.01 μm). Next, the ultrasonic cleaner was set for 10 min to ensure a smooth, clean, chemically treated surface. The ORC process was carried out in a conventional three-electrode potentiostat system, consisting of 0.1 mol/L KCl as the background solution, with infused nitrogen for 10 min to drive away oxygen from the solution. Ag/AgCl was applied as a reference electrode (RE), a

platinum wire was used as the counter electrode (CE), and Au substrate was the working electrode (WE). Cyclic voltammetry (CV) was run from −0.3 to 1.2 V for 30 cycles at a scan rate of 50 mV/s. Finally, the gold substrates were washed with deionized (DI) water, dried at room temperature, and later dried in a vacuum dryer for 24 h at room temperature.

2.4. Peptide Conjugation on the Gold Substrate

The peptide conjugation with gold substrate involved three steps. First, a 40 µL of 10 mM PEG linker (HS-PEG-NHS) diluted in DI water was dropped on the gold electrode surface. The electrode was then incubated for 6 h at 4 °C and washed three times. Second, a 40 µL of 10 mM antibody Aβ (1-28) in phosphate buffer saline (PBS) and Tween-20 (PBST) was dropped onto the PEG functionalized-surface and incubated for 12 h at 4 °C. The electrode was washed three times with PBST before being used in the subsequent step. Finally, a 20 µL Aβ (1-42) peptide with a concentration of 10^{-2}–10^{6} pg/mL in phosphate buffer saline (PBS) was dropped onto the gold surface and incubated at 4 °C for 4 h. The electrodes were then washed with PBS to remove residual peptide and dried in nitrogen (N_2) gas before use. The step-by-step workflow of the ORC nanorestructuring and surface modification is presented in Figure 1.

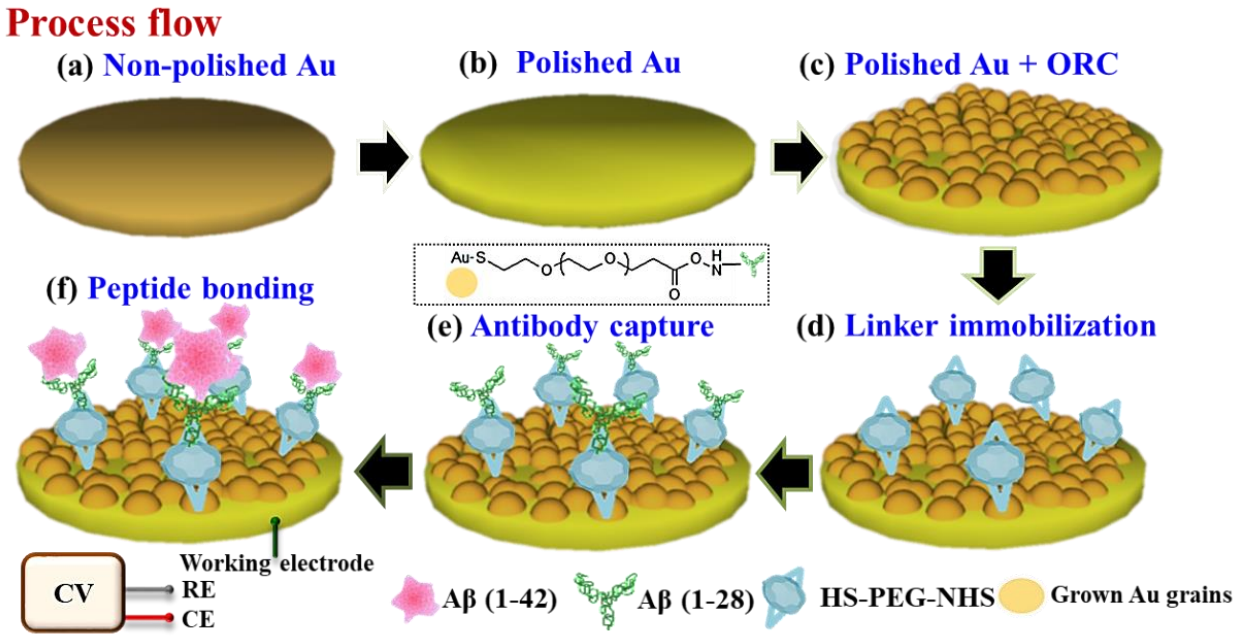

Figure 1. Schematic illustration of ORC nanorestructuring and surface modification of Au substrate for Aβ (1-42) peptide detection.

2.5. Cyclic Voltammetry (CV) Analysis for Aβ (1-42) Peptide Detection

The CV was measured using a three-electrode system consisting of Ag/AgCl as a reference, platinum wire used as the counter electrode (CE), and gold substrate as the working electrode (WE). The applied sweep voltage ranged from −0.05 to 0.4 V, at a scan rate of 50 mV/s for 24 cycles, run in a 50 mM PBS solution containing 5 mM $K_3[Fe(CN)_6]$ and 0.5 M KCl. To study Au electrode's stability produced by ORC with polishing, the CV measurement was performed under Aβ (1-42) peptide detection with 0.01 pg/mL concentration using three sensors at different cycle points.

3. Results and Discussion

3.1. ORC Treatment and Mechanism

The Au surface nanorestructuring through the ORC method has shown tremendous impacts on the surface's topological features and uniformity. In this process, a 0.1 M KCl solution was used as the background solution for all gold electrodes nanorestructuring processes as the chloride-based electrolyte solution can easily trigger the dissolution and deposition of the metal by the typical triangular voltammetry treatment [32]. All the experiments followed 30 cycles of standard ORC treatment during the fabrication. Thus, the number of cycles and scan rate would lead to different changes in the particle size and density of the Au electrode surface by ORC as verified by an optical microscope and FE-SEM in Figure 2. Under optical microscope observation in Figure 2A,B, we noticed the polishing of the Au surface with Al slurry triggered particle density and uniformity on the surface. In Figure 2C, we saw that the maximum cathode current peak appears at the scanning voltage of 0.3 V, which indicated that the gold ions were gradually being deposited back onto the surface and exhibiting activity towards oxygen reduction. A similar phenomenon was also found in the study of the roughened surface for optical application as surface-enhanced Raman spectroscopy (SERS) substrate [30,33]. It also indicated that when the degree of oxidation-reduction in the gold surface became greater, the surface changes became more rapid, thus resulting in a swifter enhancement of oxygen reduction catalytic activity [34]. Precipitation and ionization in the solution may occur. However, to some extent, they can facilitate the reduction in metallic particles size that controls the surface contour of the electrode.

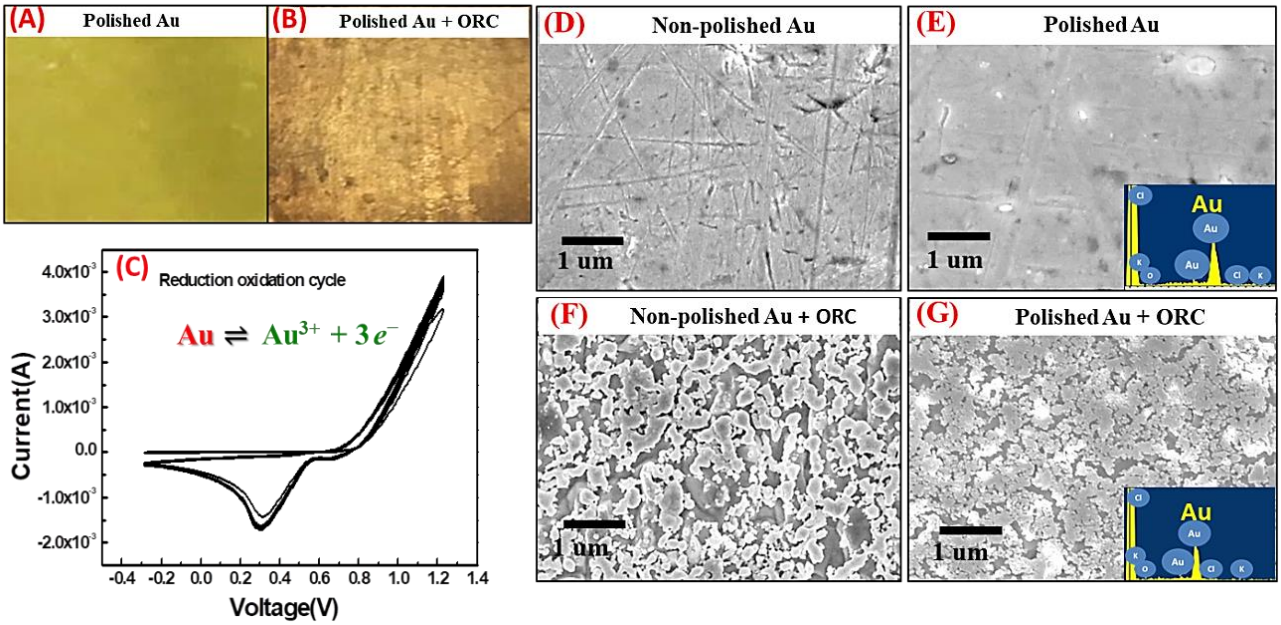

Figure 2. Optical microscopy images of Al-polished Au plate (**A**) without and (**B**) with ORC, (**C**) cyclic voltammogram of ORC process run with 30 cycles, FE-SEM figures of (**D**) non-polished and (**E**) polished Au plates without ORC, and non-polished (**F**) and polished (**G**) Au plate with ORC.

3.2. Morphological and Topological Studies of the ORC Engineered Au Substrates

The surface morphological study of the proposed techniques is presented in FE-SEM figures in Figure 2D–G. Pure gold electrodes were observed in our initial stage with and without Al polishing treatment. It is demonstrated in Figure 2D,E that the non-polished Au substrate showed harsher morphology than the polished one. The non-polished Au also showed more scratches and impurities on its surface than the polished surface carried out in ORC treatment, despite the non-polished Au initially having exhibited more contoured structure; however, after ORC, less uniform with highly clustered Au grains and lower uniformity of Au grains size were observed Figure 2F.

In contrast, in post-ORC treatment, the polished gold showed higher density and more uniform gold nanograins with a diameter of ~50 nm (Figure 2G). It is important to note that even though one of the purposes is to obtain higher surface roughness, the cleaning procedure through the polishing step is crucial to generate more uniform nanoparticle growth with higher density onto the sensing surface [35,36]. Moreover, in the energy-dispersive X-ray spectroscopy (EDX) analysis, a prominent percentage of gold over the surface is validated, as shown in the inset in Figure 2E,G.

To profoundly study the impact of the proposed ORC technique, the topological properties of the Au plates were analyzed using atomic force microscopy (AFM). The AFM was set up in the tapping mode to map the topology of the surface and check their phase characteristics. Figure 3A presents that the Ra values corresponding to the roughness factor of the surface and the RSD were calculated from three different positions of tapping mode with a dimension of 10μm × 10μm for each measurement. The effects of Al polishing in AFM analysis affirms the findings in the optical microscope and FE-SEM figures as represented by higher surface roughness of the non-polished Au substrate with an initial Ra value of 46.1% than the polished Au, which only shows about 4% of Ra value. Being followed by the ORC process, both non-polished and polished substrates exhibited a higher surface roughness than the surface properties prior to ORC, as expressed in the RSD of the Ra values of 55.4% and 5.9%, respectively. However, surface roughness is not the sole parameter for signal augmentation and well-propagation in the nanorestructuring of active surface sites. The other essential factor is the particles' density and uniformity, giving rise to the surface roughness. The highly uniform Au grain size provides a major landing point for the probe biomolecules immobilization, leading to the effective binding of the counterpart molecules. In the height profile analysis depicted in Figure 3B,C, the non-polished Au showed the propensity to generate irregular particles height with a high disparity, around 50–500 nm, and an average length of approximately 50–500 nm.

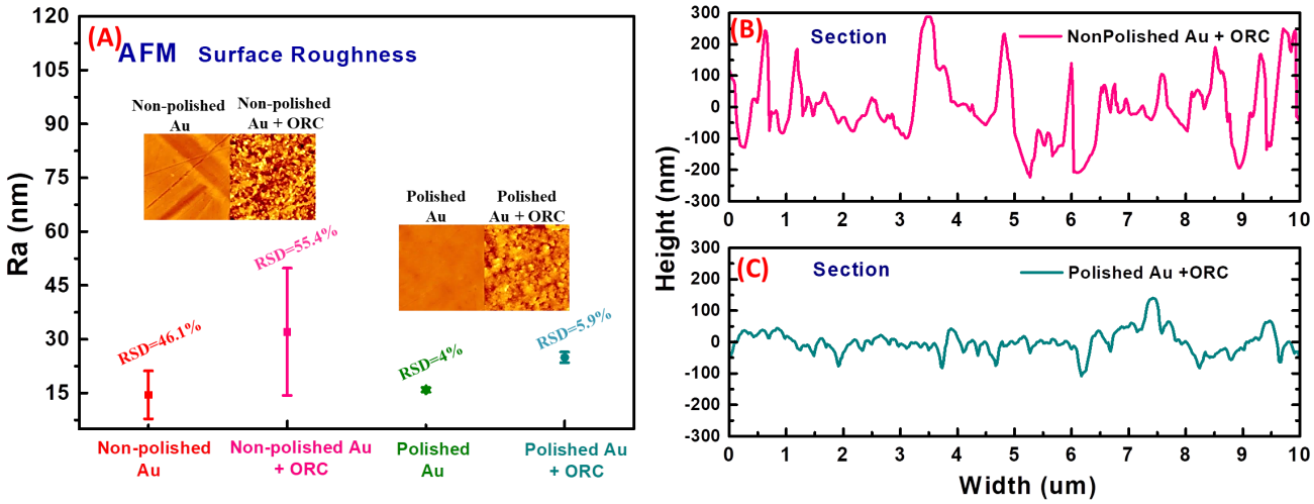

Figure 3. (**A**) Surface roughness profiles from AFM analysis of the Au substrate having undergone different treatments, and the height profile of (**B**) non-polished and (**C**) polished Au surface after ORC treatment.

Polishing treatment had significantly generated more uniform Au particles size and density after ORC treatment by the average height of about 50–100 nm and the length of approximately 50–150 nm over the Au substrate (Figure 3C). The outcomes signify the crucial role of polishing and cleaning the substrate to create a homogenous foundation and particle size control for Au growth [34]. Moreover, the largely homogenous surface resulting from polishing facilitates the well-scattered penetration of Au ions during the

electrochemical ORC, where such actions will likely be hindered in the randomly roughened and dirty non-polished surface.

3.3. Electroactive Surface Area of the ORC Nanorestructured Au Substrate

To deeply comprehend the impact of polishing and ORC treatment on the Au substrate, the study was conducted towards calculating the surface area based on the cyclic voltammetry analysis. Figure 4A,B represent the cyclic voltammograms of a 50 mM PBS solution containing 5 mM $K_3[Fe(CN)_6]/K_4[Fe(CN)_6]$ and 0.5 M KCl mixture for the polished gold surface with and without ORC treatment. The scan rate and the peak current gradually increased proportionally to $\nu^{1/2}$ on gold surfaces both treated with and without ORC, as displayed in Figure 4C,D, implying that the reaction was under a quasi-reversible process typically found in Au nanoparticles studies for nanopatterning [37,38]. However, the impact of morphological and topological characters after ORC treatment in generating more current response through the oxidation and reduction reaction of ferri/ferrocyanide ions onto the surface was conspicuously displayed in more significant current-based peak-to-peak separation in Figure 4B, as well as being indicative of the more substantial diffusion coefficient. The electroactive surface area and diffusion coefficient were calculated using the mechanism based on electron transfer via the Randles–Sevcik equation [39–41]:

$$i_p = (2.69 \times 10^5)\, n^{3/2} A D^{1/2} C \upsilon^{1/2} \quad (1)$$

where i_p is the peak current, n is the number of electrons transferred, A is the active area of the working electrode, D is the standard diffusion coefficient for the used redox probe $K_3Fe(CN)_6$, which is equal to 7.6×10^{-6} cm^2/s, and C is the concentration of the redox species, υ is the scan rate in solution. The quantification confirms the higher electroactive area of the polished Au surface followed by ORC treatment than the substrate treated by only polishing a step with the value of 0.76 cm^2 and 0.66 cm^2, respectively, concerning the geometrical area of 38.465 mm^2 (electrode diameter = 7 mm) for the Au electrode before applying the polishing method. In principle, a ~15% increment of the electroactive surface area through the ORC process is projected to favor higher electron conversion and mass transfer on the working electrode to amplify the sensing sensitivity.

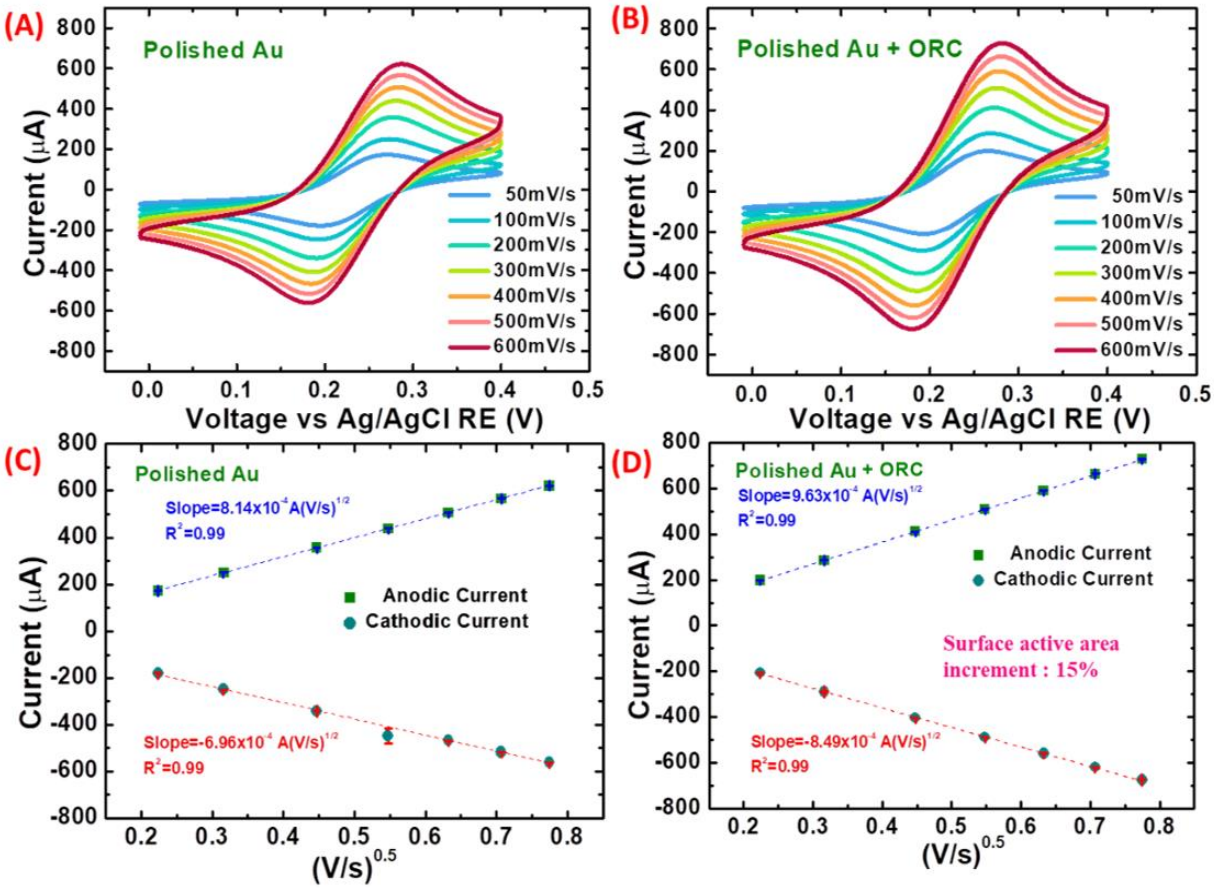

Figure 4. Cyclic voltammograms (CV) run between 0 and 0.4 V in 5 mM $K_3[Fe(CN)_6]/K_4[Fe(CN)_6]$ and 0.5 M KCl at various scan rates of polished Au surface (**A**) without and (**B**) with ORC treatment. The relation of the anodic peak current on the scan rate square root with the calculated correlation coefficient for polished Au surface (**C**) without and (**D**) with ORC treatment.

3.4. Electrochemical Detection of Aβ (1-42) Peptide Using ORC Nanorestructured Au Substrate

Alzheimer's disease (AD) is typically diagnosed from the occurrence of protein lesions in the brain, and the β-amyloid Aβ (1-42) protein has been shown to be much higher in the incidence of AD patients. Among other AD biomarkers, Aβ (1-42) protein has been highly noted as an important precursor since 1987 [42]. In this work, as a proof of concept in early detection of AD, the ORC engineered Au substrate was applied as an electrochemical sensor. The uniformly grown Au grains would promote the effective adhesion of protein Aβ (1-28) probes in a high surface area and control the density of the probe molecules, which later provide high binding efficiency with target peptide. The use of SH-PEG-NHS on anchoring the antibody Aβ (1-42) facilitates a straightforward and stable crosslinking process with no other activation steps required. The SH-PEG-NHS is a common linker used in modifying proteins and drugs since the NHS ester reacts with the primary amine group of antibody/proteins at pH 7–8.5 to form a stable amide bond [43,44]. It can also suppress the non-specific binding of charged molecules to the modified surfaces. PEGylation can increase solubility and stability and reduce immunogenicity of peptides and proteins. A similar procedure has been reported before for the immobilization of α-synuclein (αS) protein on a gold surface in near-field effect detection [45,46]. The detection of Aβ (1-42) protein and corresponding CV analysis for the detection of 10^{-2} to 10^{6} pg/mL is displayed in Figure 5. It is also observed that in the polished Au substrate without ORC in Figure 5A, the CV curves did not show complete redox peaks at the given voltage range.

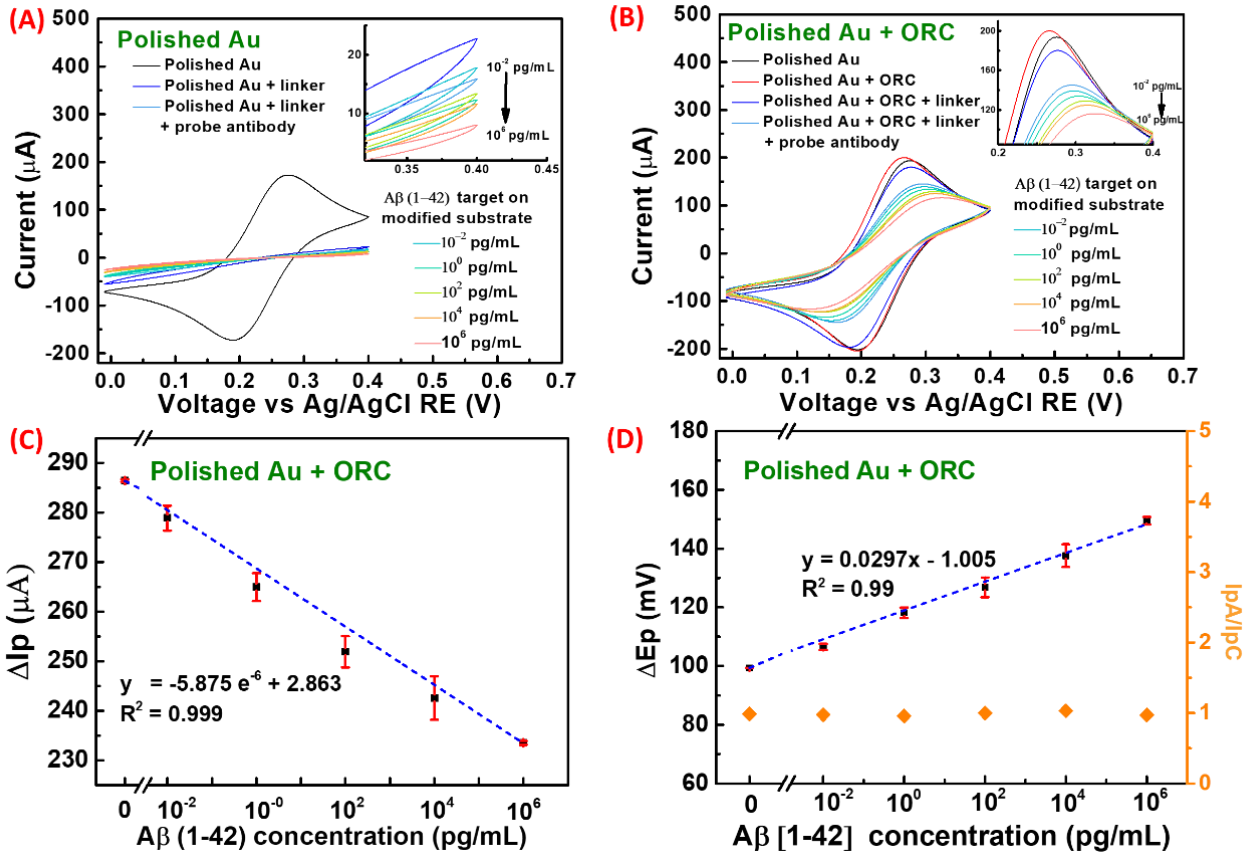

Figure 5. Cyclic voltammogram (CV) of polished gold (**A**) without and (**B**) with ORC for of Aβ (1-42) peptide detection. Inset shows the enlarged anodic peak current (ΔIp) trend of the CV in Aβ (1-42) peptide detection, which gradually decreases with increasing peptide concentration, and sensitivity plot of the (**C**) peak current (ΔIp) and (**D**) peak voltage (ΔEp) and IpA and IpC ratio of the polished Au with ORC treatment for Aβ (1-42) peptide detection.

On the contrary, as displayed in Figure 5B, in the polished Au substrate followed by the ORC treatment, the peak currents in cyclic voltammetry gradually decreased as the target Aβ (1-42) peptide concentration was added onto the interface. The electron repulsion can decipher this phenomenon with the negative ions of ferri/ferrocyanide redox dye in the applied electrochemical cell caused by higher loads of negatively charged peptides as the target increased with the negative ions of ferri/ferrocyanide redox dye in the used electrochemical cell, which also involved in the DNA detection studies [37]. The trend of the current signals in the Aβ (1-42) peptide detection is presented in the value of ΔI_p as the difference between the anodic peak (I_{pa}) and cathodic peak (I_{pc}) using three different substrates out of 24 cycles with standard deviation (Figure 5C). Subsequently, concerning the cyclic voltammogram behavior, the higher the analytical signal change, the more free binding sites decreased [47]. However, the values of ΔI_p will be the consequence of the surface coverage between the gold surface and $[Fe(CN)_6]^{3-/4-}$ contact area during Aβ (1-42) bonding resulting in reduced electron transfer kinetics. An extensive dynamic range of 10^{-2} to 10^6 pg/mL was performed in the Aβ (1-42) peptide detection in this study and tremendously favors the clinical cutoff for this biomarker, which is more than 40 pg/mL in the AD patients' blood plasma [48]. Furthermore, the limit of detection (LoD) is an essential benchmark for noting the potency of the ORC modified Au substrate in enabling rapid and accurate screening for early diagnosis of AD. The LoD calculation was carried out by comparing the three instances of standard deviation of the zero concentration of target, divided by the sensitivity of the sensing response, which finally re-

sults in the value of 10.4 fg/mL. The obtained LoD in this work also denotes that the ORC nanorestructured Au does not intrinsically restrict the sensitivity of the biosensor. The dependence of anode and cathode peak potential ($E_{pa} - E_{pc} = \Delta E_p$) of protein is shown in Figure 5D. The potential peak becomes larger as the concentration of the protein increases when the anode shift to a positive voltage and the cathode shift to a negative voltage [33]. This means that the reversibility of $[Fe(CN)_6]/K_4[Fe(CN)_6]$ requires a higher potential to drive the complete transfer of electrons near the gold surface [49] since the HS-PEG-NHS linker, Aβ (1-28) probe and Aβ (1-42) peptide target were attached significantly, and hence, added a potential energy barrier onto the interface.

Additionally, the presence of highly negatively charged proteins would in return shift the anodic potential peak towards more positive voltage values to fulfill the neutrality point. Besides, Figure 5D represents the redox cycle stability. The IpA and IpC ratio for each measurement was recorded with the value of nearly one, referring to reversible couples of the oxidation-reduction reaction. This indicated that the modified electrode has a good reversibility in our electrochemical sweep cycle [50].

The stability of the ORC nanorestructured Au substrate in the measurement of Aβ (1-42) peptide was studied in the ΔIp and ΔEp variation against numbers of cycles. In Figure 6A,B, in the detection of target peptide with a range of concentration under a series of cycle numbers, the current and voltage signals did not vary as much, as shown by a significant coefficient of variation (CV) value of less than 0.5% resulting from three different substrates at various numbers of cycles, respectively, in all cycles tested. This reflects that the sensor possesses excellent stability even for such high cycling set up and with lower Aβ (1-42) concentrations and that the solid biomolecular adhesion and interaction were still preserved despite highly repeated measurements. Moreover, it is noteworthy that the stability confirms the reproducibility of the Au grains over the substrate created through the ORC after a repetitive measurement, which concomitantly counters the issue of deposited metal exfoliation as the effect of high cycle numbers. When compared with the previously published works of literature that have highlighted the surface engineering of sensor and platform structures for Aβ proteins detection, shown in Table 1, the ORC nanorestructured Au electrode performs outstandingly, surpassing previous work on points such as the ease and cost-effectiveness of sensor fabrication, wider dynamic range, and low LoD.

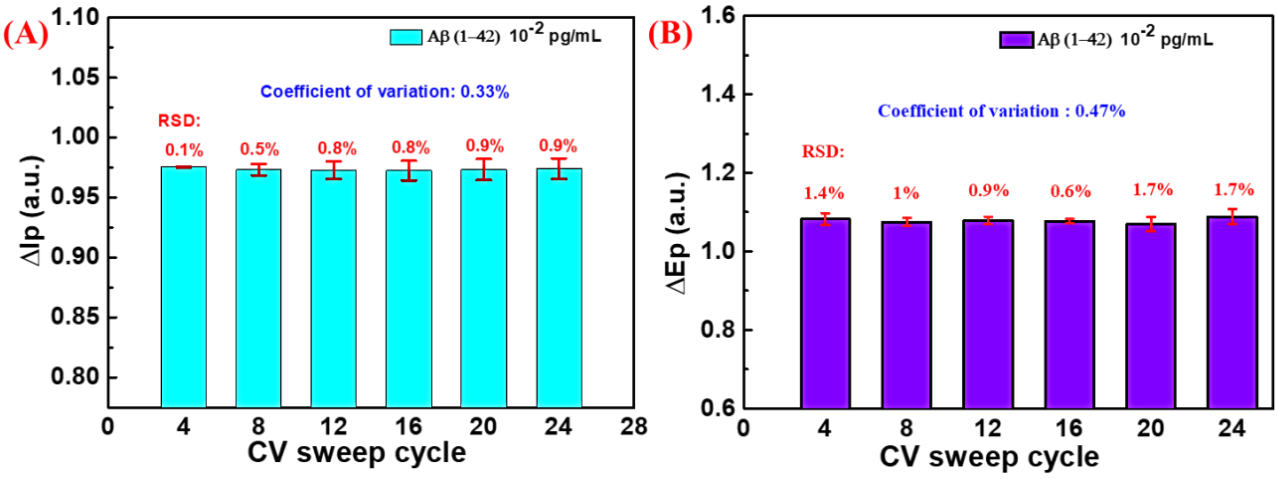

Figure 6. Stability of (**A**) ΔI_p and (**B**) ΔE_p of Aβ (1-42) peptide detection with 0.01 pg/mL concentration using three sensors at different cycle points run in CV between 0 and 0.4 V at a scan rate of 50 mV/s in 5 mM $K_3[Fe(CN)_6]/K_4[Fe(CN)_6]$ and 0.5 M KCl using polished, and ORC treated gold sheet plate.

Table 1. Performance and features comparison: previously published Aβ (1-42) sensor versus the proposed ORC modified Au substrate.

Detection Route	Final Structure	Nanopatterning Approach	Detection Range	LoD	Ref
Fluorescent signals	Microfluidic + Magnetic beads	PDMS and magnetic beads	0.5–1 nM	N/A	[51]
Electrochemical sensor	Fern leaves-like gold nanostructure	Electrochemical	0.002–1.28 ng/mL	0.4 pg/mL	[52]
Optical Sensor	Microfluidic	E-beam evaporation and lithography	3.9 pg–500 pg/mL	N/A	[53]
Square Wave Voltammetry (SWV)	AuNPs/MPA/Au /Synthesis and Electro deposition	Chemical synthesis and electro deposition	10–1000 pg mL^{-1}	5.2 pg mL^{-1}	[54]
Electrochemical Impedance Spectroscopy (EIS)	Gold/AuNPs	Chemical synthesis	0.1 nM–5uM	45 pM	[55]
Linear Sweep Voltammetry (LSV)	Gold/AuNPs	Chemical synthesis	0.01–200 nM	6 pM	[56]
EIS, SWV	PANI/Au	Screen printing	0.25–0.2 ng/mL	4.4×10^{-11} M	[47]
Dual Pulsed Voltammetry (DPV), CV	Carbon/AuNPs	Chemical synthesis	100 fM–25 pM.	N/A	[57]
EIS, CV	Poly(curcumin-Ni)	Electrochemical	0.001–5 nM	0.001 nM	[58]
DPV, CV	Glassy carbon/AuNPs + Cu-MOF	Chemical synthesis and electro deposition	0.001–5nM	0.45 nmol L^{-1}	[59]
Electro-chemilumines cence	Glassy carbon/AuNPs	Chemical synthesis and deposition	0.1 pg/mL–10 ng/mL	19.95 fg/mL	[60]
Field Effect Transistor (FET)	SiO_2 FET substrate	n/a	100 pM–10 μM.	N/A	[61]
CV system	**Au roughened substrate**	**Electrochemical ORC**	**0.01–10^6 pg/mL**	**10.4 fg/mL**	**This Work**

4. Conclusions

A simple ORC-based technique for topological improvement through nanorestructuring of Au plate was performed for early detection of AD through Aβ (1-42) peptide biomarker screening on an electrochemical sensor setup. The polishing strategy played an important role in determining the final structure of the ORC modified substrate since it provided the foundation of the nanoarchitecture. The ORC nanorestructuring on a polished substrate was proven effective in generating a high density of Au nanograins with more uniform particle height and size than the treatment without polishing. Interestingly as a proof of concept, with a simple and cost-effective ORC method, the electroactive surface area of the sensor could be significantly enlarged, favoring a wide dynamic range of Aβ (1-42) peptide detection with considerably low LoD. Furthermore, the stability and reproducibility of the ORC-modified Au substrate were outstandingly retained in highly repetitive measurements. Overall, we envisage that the ORC-based nanopatterning provides a facile, cheap, and easy top-down strategy for large-scale biosensor development in interdisciplinary areas.

Author Contributions:

Funding: This research is financially supported by the Ministry of Science and Technology, Taiwan under project number MOST: MOST 110-2221-E-182 -043 -MY3, 109-2221-E-182 -013 -MY3, 110-2119-M-492-002 –MBK, 110-2622-8-182-001 -TS1.

Institutional Review Board Statement:

Informed Consent Statement:

Data Availability Statement:

Conflicts of Interest: The authors declare no conflict of interest.

References

1. Michelle, M.; Prashanthi, V.; Walter, R. Clinical epidemiology of Alzheimer's disease: Assessing sex and gender differences. *Clin. Epidemiol.* **2014**, *6*, 37–48.
2. Kaushik, A.; Jayant, R.D.; Tiwari, S.; Vashist, A.; Nair, M. Nano-biosensors to detect beta-amyloid for Alzheimer's disease management. *Biosens. Bioelectron.* **2016**, *80*, 273–287, doi:10.1016/j.bios.2016.01.065.
3. Kaushik, A.; Shah, P.; Vabbina, P.K.; Jayant, R.D.; Tiwari, S.; Vashist, A.; Yndart, A.; Nair, M. A label-free electrochemical immunosensor for beta-amyloid detection. *Anal. Methods* **2016**, *8*, 6115–6120.
4. C., R.; R., M. Alzheimer disease: Epidemiology, diagnostic criteria, risk factors and biomarkers. *Biochem. Pharmacol.* **2014**, *88*, 640–651.
5. Htike, T.T.; Mishra, S.; Kumar, S.; Padmanabhan, P.; Gulyás, B. Peripheral Biomarkers for Early Detection of Alzheimer's and Parkinson's Diseases. *Mol. Neurobiol.* **2019**, *56*, 2256–2277.
6. Wang, W.F.; Chiu, P.Y.; Lin, Y. Te; Hu, C.J.; Fuh, J.L.; Yang, Y.H. Registration of Alzheimer's disease in Taiwan: Patient and informant. *Am. J. Alzheimers. Dis. Other Demen.* **2014**, *29*, 18–22.
7. Fuh, J.-L.; Wang, S.-J. Dementia in Taiwan: Past, present, and future. *Acta Neurol. Taiwan.* **2008**, *17*, 153–161.
8. Liu C.K.; Lai C.L.; Tai C.T.; Lin R.T.; Yen Y.Y.; Howng S.L. Incidence and subtypes of dementia in southern Taiwan. Impact of socio- demographic factors. *Neurology* **1998**, *50*, 1572–1579.
9. Dragomir, A.; Vrahatis, A.G.; Bezerianos, A. A network-based perspective in Alzheimer's disease: Current state and an integrative framework. *IEEE J. Biomed. Heal. Informatics* **2019**, *23*, 14–25.
10. Teleanu, D.M.; Negut, I.; Grumezescu, V.; Grumezescu, A.M.; Teleanu, R.I. Nanomaterials for drug delivery to the central nervous system. *Nanomaterials* **2019**, *9*, 371.
11. Panzarini, E.; Mariano, S.; Tacconi, S.; Carata, E.; Tata, A.M.; Dini, L. Novel therapeutic delivery of nanocurcumin in central nervous system related disorders. *Nanomaterials* **2021**, *11*, 1–30.
12. Nortley, R.; Korte, N.; Izquierdo, P.; Hirunpattarasilp, C.; Mishra, A.; Jaunmuktane, Z.; Kyrargyri, V.; Pfeiffer, T.; Khennouf, L.; Madry, C.; et al. Amyloid β oligomers constrict human capillaries in Alzheimer's disease via signaling to pericytes. *Science (80-.).* **2019**, *365*, eaav9518.
13. Esparza, T.J.; Wildburger, N.C.; Jiang, H.; Gangolli, M.; Cairns, N.J.; Bateman, R.J.; Brody, D.L. Soluble amyloid-beta aggregates from human Alzheimer's disease brains. *Sci. Rep.* **2016**, *6*, 1–16.
14. Carneiro, P.; Morais, S.; Pereira, M.C. Nanomaterials towards biosensing of Alzheimer's disease biomarkers. *Nanomaterials* **2019**, *9*, 1663.
15. Desai, U.; Kirson, N.Y.; Mehta, N.; Wen, J.; Sheng, Y.; Ye, W.; Andrews, J.S. Trends in Health Service Use and Potentially Avoidable Hospitalizations Prior To Alzheimer'S Disease Diagnosis: a Matched, Retrospective Study of U.S. Medicare Beneficiaries. *Alzheimer's Dement.* **2019**, *11*, 125–135.

16. Vemuri, P.; Jack, C.R. Role of structural MRI in Alzheimer's disease. *Alzheimer's Res. Ther.* **2010**, *2*, 23.
17. Ossenkoppele, R.; Schonhaut, D.R.; Schöll, M.; Lockhart, S.N.; Ayakta, N.; Baker, S.L.; O'Neil, J.P.; Janabi, M.; Lazaris, A.; Cantwell, A.; et al. Tau PET patterns mirror clinical and neuroanatomical variability in Alzheimer's disease. *Brain* **2016**, *139*, 1551–1567.
18. Bilgel, M.; Jedynak, B.M. Predicting time to dementia using a quantitative template of disease progression. *Alzheimer's Dement. Diagnosis, Assess. Dis. Monit.* **2019**, *11*, 205–215.
19. Wise, E.A.; Rosenberg, P.B.; Lyketsos, C.G.; Leoutsakos, J.M. Time course of neuropsychiatric symptoms and cognitive diagnosis in National Alzheimer's Coordinating Centers volunteers. *Alzheimer's Dement. Diagnosis, Assess. Dis. Monit.* **2019**, *11*, 333–339.
20. Doane, T.L.; Burda, C. The unique role of nanoparticles in nanomedicine: Imaging, drug delivery and therapy. *Chem. Soc. Rev.* **2012**, *41*, 2885–2911.
21. Zhang, B.; Tang, X.; Zhang, B.; Xiao, C.; Zhou, H.; Wang, X.; He, D. Carbon nanotube template synthesis of hierarchical NiCoO2 composite for non-enzyme glucose detection Sensors and Actuators B : Chemical Carbon nanotube template synthesis of hierarchical NiCoO 2 composite for non-enzyme glucose detection. *Sensors Actuators B. Chem.* **2016**, *222*, 232–239.
22. El Mel, A.A.; Boukli-Hacene, F.; Molina-Luna, L.; Bouts, N.; Chauvin, A.; Thiry, D.; Gautron, E.; Gautier, N.; Tessier, P.Y. Unusual dealloying effect in gold/copper alloy thin films: The role of defects and column boundaries in the formation of nanoporous gold. *ACS Appl. Mater. Interfaces* **2015**, *7*, 2310–2321.
23. Tajabadi, M.T.; Sookhakian, M.; Zalnezhad, E.; Yoon, G.H.; Hamouda, A.M.S.; Azarang, M.; Basirun, W.J.; Alias, Y. Electrodeposition of flower-like platinum on electrophoretically grown nitrogen-doped graphene as a highly sensitive electrochemical non-enzymatic biosensor for hydrogen peroxide detection. *Appl. Surf. Sci.* **2016**, *386*, 418–426.
24. Deng, Y.; Huang, W.; Chen, X.; Li, Z. Facile fabrication of nanoporous gold film electrodes. *Electrochem. commun.* **2008**, *10*, 810–813.
25. Zhong, G.; Lan, R.; Zhang, W.; Fu, F.; Sun, Y.; Peng, H.; Chen, T.; Cai, Y.; Liu, A.; Lin, J.; et al. Sensitive electrochemical immunosensor based on three-dimensional nanostructure gold electrode. *Int. J. Nanomedicine* **2015**, *10*, 2219–2228.
26. Asnavandi, M.; Zhao, C. Autologous growth of nickel oxyhydroxides with: In situ electrochemical iron doping for efficient oxygen evolution reactions. *Mater. Chem. Front.* **2017**, *1*, 2541–2546.
27. Zhu, G.; He, Z.; Chen, J.; Zhao, J.; Feng, X.; Ma, Y.; Fan, Q.; Wang, L.; Huang, W. Highly conductive three-dimensional MnO2-carbon nanotube-graphene-Ni hybrid foam as a binder-free supercapacitor electrode. *Nanoscale* **2014**, *6*, 1079–1085.
28. Sheng, Q.; Mei, H.; Wu, H.; Zhang, X.; Wang, S. A non-enzymatic amperometric glucose sensor based on three dimensional nanostructure gold electrode. *Sensors Actuators B. Chem.* **2015**, *212*, 7277.
29. Wang, W.; Huang, Y.F.; Liu, D.Y.; Wang, F.F.; Tian, Z.Q.; Zhan, D. Electrochemically roughened gold microelectrode for surface-enhanced Raman spectroscopy. *J. Electroanal. Chem.* **2016**, *779*, 126–130, doi:10.1016/j.jelechem.2016.04.008.
30. Liu, Y.C.; Hwang, B.J.; Jian, W.J. Effect of preparation conditions for roughening gold substrate by oxidation-reduction cycle on the surface-enhanced Raman spectroscopy of polypyrrole. *Mater. Chem. Phys.* **2002**, *73*, 129–134.
31. Bailey, M.R.; Pentecost, A.M.; Selimovic, A.; Martin, R.S.; Schultz, Z.D. Sheath-flow microfluidic approach for combined surface enhanced Raman scattering and electrochemical detection. *Anal. Chem.* **2015**, *87*, 4347–4355.

32. Ivanovskaya, A.N.; Belle, A.M.; Yorita, A.M.; Qian, F.; Chen, S.; Tooker, A.; Lozada, R.G.; Dahlquist, D.; Tolosa, V. Electrochemical Roughening of Thin-Film Platinum for Neural Probe Arrays and Biosensing Applications. *J. Electrochem. Soc.* **2018**, *165*, G3125–G3132.
33. Liu, Y.C.; Wang, C.C.; Tsai, C.E. Effects of electrolytes used in roughening gold substrates by oxidation-reduction cycles on surface-enhanced Raman scattering. *Electrochem. commun.* **2005**, *7*, 1345–1350.
34. Lim, T.; Kim, J. Effect of electrochemical oxidation-reduction cycles on surface structures and electrocatalytic oxygen reduction activity of Au electrodes. *J. Korean Chem. Soc.* **2016**, *60*, 310–316, doi:10.5012/jkcs.2016.60.5.310.
35. Kai, T.; Chen, S.; Monterroso, E.; Zhou, F. Continuous nanoflow-scanning electrochemical microscopy: Voltammetric characterization and application for accurate and reproducible imaging of enzyme-labeled protein microarrays. *Anal. Chem.* **2015**, *87*, 4523–4529.
36. Xu, Y.; Ke, X.; Yu, C.; Liu, S.; Zhao, J.; Cui, G.; Higgins, D.; Chen, Z.; Li, Q.; Wu, G. A strategy for fabricating nanoporous gold films through chemical dealloying of electrochemically deposited Au-Sn alloys. *Nanotechnology* **2014**, *25*, 445602.
37. Purwidyantri, A.; Chen, C.-H.; Chen, L.-Y.; Chen, C.-C.; Luo, J.-D.; Chiou, C.-C.; Tian, Y.-C.; Lin, C.-Y.; Yang, C.-M.; Lai, H.-C.; et al. Speckled ZnO Nanograss Electrochemical Sensor for Staphylococcus epidermidis Detection. *J. Electrochem. Soc.* **2017**, *164*, B205–B211.
38. Purwidyantri, A.; Lai, H.-C.H.-C.; Tsai, S.-H.S.-H.; Luo, J.-D.; Chiou, C.-C.C.-C.; Tian, Y.-C.; Cheng, C.-H.; Lin, Y.-T.; Lai, C.-S.C.-S.; Chengh, C.-H.; et al. Sensing performance of fibronectin-functionalized Au-EGFET on the detection of S. epidermidis biofilm and 16S rRNA of infection-related bacteria in peritoneal dialysis. *Sensors Actuators B Chem.* **2015**, *217*, 92–99, doi:10.1016/j.snb.2014.11.017.
39. Pandey, R.R.; Alshahrani, H.S.; Krylyuk, S.; Williams, E.H.; Davydov, A. V.; Chusuei, C.C. Electrochemical Detection of Acetaminophen with Silicon Nanowires. *Electroanalysis* **2018**, *30*, 886–891.
40. Rizk, M.; Sultan, M.A.; Taha, E.A.; Attia, A.K.; Abdallah, Y.M. Sensitive validated voltammetric determination of apixaban using a multi-walled carbon nanotube-modified carbon paste electrode application to a drug product and biological sample. *Anal. Methods* **2017**, *9*, 2523–2534.
41. Lu, Y.J.; Purwidyantri, A.; Liu, H.L.; Wang, L.W.; Shih, C.Y.; Pijanowska, D.G.; Yang, C.M. Photoelectrochemical Detection of β-amyloid Peptides by a TiO2 Nanobrush Biosensor. *IEEE Sens. J.* **2020**, *20*, 6248–6255, doi:10.1109/JSEN.2020.2976561.
42. Tanzi, R.E.; George-Hyslop, P.H.S.; Haines, J.L.; Polinsky, R.J.; Nee, L.; Foncin, J.F.; Neve, R.L.; McClatchey, A.I.; Conneally, P.M.; Gusella, J.F. The genetic defect in familial Alzheimer's disease is not tightly linked to the amyloid β-protein gene. *Nature* **1987**, *329*, 156–157.
43. Hamley, I.W. PEG − Peptide Conjugates. *Biomacromolecules* **2014**, *15*, 1543−1559.
44. Mills, S.C.; Starr, N.E.; Bohannon, N.J.; Andrew, J.S. Chelating Agent Functionalized Substrates for the Formation of Thick Films via Electrophoretic Deposition. *Front. Chem.* **2021**, *9*, 703528, doi:10.3389/fchem.2021.703528.
45. Jarrell, D.K.; Vanderslice, E.J.; Lennon, M.L.; Lyons, A.C.; VeDepo, M.C.; Jacot, J.G. Increasing salinity of fibrinogen solvent generates stable fibrin hydrogels for cell delivery or tissue engineering. *PLoS One* **2021**, *16*, e0239242, doi:10.1371/journal.pone.0239242.
46. Fallah, M.A.; Hauser, K. Immobilization approaches can affect protein dynamics: A surface-enhanced infrared spectroscopic study on lipid-protein interactions. *Biomater. Sci.* **2019**, *7*, 3204–3212, doi:10.1039/c9bm00140a.

47. Moreira, F.T.C.; Sales, M.G.F. Smart naturally plastic antibody based on poly(α-cyclodextrin) polymer for β-amyloid-42 soluble oligomer detection. *Sensors Actuators, B Chem.* **2017**, *240*, 229–238.
48. Bateman, R.J.; Fagan, A.M.; Holtzman, D.M.; Santacruz, A.; Buckles, V.; Oliver, A.; Moulder, K.; Morris, J.C.; Xiong, C.; Xie, X.; et al. Clinical and biomarker changes in dominantly inherited Alzheimer's disease. *N. Engl. J. Med.* **2012**, *367*, 795–804.
49. De Lima, F.; Maia, G. Oxidized/reduced graphene nanoribbons facilitate charge transfer to the Fe(CN)63-/Fe(CN)64-redox couple and towards oxygen reduction. *Nanoscale* **2015**, *7*, 6193–6207.
50. Radhi, M.M.; Alosfur, F.K.M.; Ridha, N.J. Voltammetric Characterization of Grafted Polymer Modified with ZnO Nanoparticles on Glassy Carbon Electrode. *Russ. J. Electrochem.* **2018**, *54*, 27–32.
51. Mai, T.D.; Ferraro, D.; Aboud, N.; Renault, R.; Serra, M.; Tran, N.T.; Viovy, J.L.; Smadja, C.; Descroix, S.; Taverna, M. Single-step immunoassays and microfluidic droplet operation: Towards a versatile approach for detection of amyloid-β peptide-based biomarkers of Alzheimer's disease. *Sensors Actuators, B Chem.* **2018**, *255*, 2126–2135.
52. Negahdary, M.; Heli, H. An ultrasensitive electrochemical aptasensor for early diagnosis of Alzheimer's disease, using a fern leaves-like gold nanostructure. *Talanta* **2019**, *198*, 510–517.
53. Song, C.; Deng, P.; Que, L. Rapid multiplexed detection of beta-amyloid and total-tau as biomarkers for Alzheimer's disease in cerebrospinal fluid. *Nanomedicine Nanotechnology, Biol. Med.* **2018**, *14*, 1845–1852.
54. Carneiro, P.; Loureiro, J.; Delerue-Matos, C.; Morais, S.; do Carmo Pereira, M. Alzheimer's disease: Development of a sensitive label-free electrochemical immunosensor for detection of amyloid beta peptide. *Sensors Actuators, B Chem.* **2017**, doi:10.1016/j.snb.2016.07.181.
55. Xia, N.; Wang, X.; Yu, J.; Wu, Y.; Cheng, S.; Xing, Y.; Liu, L. Design of electrochemical biosensors with peptide probes as the receptors of targets and the inducers of gold nanoparticles assembly on electrode surface. *Sensors Actuators, B Chem.* **2017**, *239*, 834–840.
56. Xing, Y.; Feng, X.Z.; Zhang, L.; Hou, J.; Han, G.C.; Chen, Z. a sensitive and selective electrochemical biosensor for the determination of beta-amyloid oligomer by inhibiting the peptide-triggered in situ assembly of silver nanoparticles. *Int. J. Nanomedicine* **2017**, *12*, 3171–3179.
57. Diba, F.S.; Kim, S.; Lee, H.J. Electrochemical immunoassay for amyloid-beta 1–42 peptide in biological fluids interfacing with a gold nanoparticle modified carbon surface. *Catal. Today* **2017**, *295*, 41–47.
58. Qin, J.; Park, J.S.; Jo, D.G.; Cho, M.; Lee, Y. Curcumin-based electrochemical sensor of amyloid-B oligomer for the early detection of Alzheimer's disease. *Sensors Actuators, B Chem.* **2018**, *273*, 1593–1599.
59. Zhou, Y.; Li, C.; Li, X.; Zhu, X.; Ye, B.; Xu, M. A sensitive aptasensor for the detection of β-amyloid oligomers based on metal-organic frameworks as electrochemical signal probes. *Anal. Methods* **2018**, *10*, 4430–4437.
60. Jia, Y.; Yang, L.; Feng, R.; Ma, H.; Fan, D.; Yan, T.; Feng, R.; Du, B.; Wei, Q. MnCO 3 as a new electrochemiluminescence emitter for ultrasensitive bioanalysis of β-Amyloid 1-42 oligomers based on site-directed immobilization of antibody. *ACS Appl. Mater. Interfaces* **2019**, *11*, 7157–7163.
61. Hideshima, S.; Wustoni, S.; Kobayashi, M.; Hayashi, H.; Kuroiwa, S.; Nakanishi, T.; Osaka, T. Effect of human serum on the electrical detection of amyloid-β fibrils in biological environments using azo-dye immobilized field effect transistor (FET) biosensor. *Sens. Bio-Sensing Res.* **2018**, *17*, 25–29, doi:10.1016/j.sbsr.2018.01.003.